RSC Advances

Cite this: *RSC Advances*, 2012, **2**, 5329–5336

www.rsc.org/advances

PAPER

Vertically-aligned carbon nanotube membranes for hydrogen separation

Lei Ge,[a] Li Wang,[a] Aijun Du,[b] Meng Hou,[c] Victor Rudolph[a] and Zhonghua Zhu*[a]

Received 5th January 2012, Accepted 27th March 2012
DOI: 10.1039/c2ra00031h

Vertically-aligned carbon nanotube membranes have been fabricated and characterized and the corresponding gas permeability and hydrogen separation were measured. The carbon nanotube diameter and areal density were adjusted by varying the catalyst vapour concentration (Fe/C ratio) in the mixed precursor. The permeances are one to two magnitudes higher than the Knudsen prediction, while the gas selectivities are still in the Knudsen range. The diameter and areal density effects were studied and compared, the temperature dependence of permeation is also discussed. The results confirm the existence of non-Knudsen transport and that surface adsorption diffusion may affect the total permeance at relative low temperature. The permeance of aligned carbon nanotube membranes can be improved by increasing areal density and operating at an optimum temperature.

1. Introduction

Vertically-aligned carbon nanotubes (VACNT), due to their ordered structure and anisotropic properties, have been receiving considerable attention for a variety of potential applications, such as field emission devices,[1,2] composites,[3] energy storage[4] and conversion,[5] and separation membranes.[6,7] Vertically-aligned CNT membranes, with ordered cylinder pores (diameters typically 1–2 nm with single-walled nanotubes and 5–20 nm with multi-walled nanotubes) and smooth carbon layers, may provide a separation method that uses less energy for applications such as selective separation of nanoparticles, microorganisms, or bimolecules.[8–12] In addition, CNTs can be turned into "gate-keepers" by functionalising the CNT tips, providing additional selectivity.[13] As a whole, CNT membranes show very desirable characteristics including both selective affinities for adsorbing molecules and high diffusion speed, presenting a potentially attractive platform for analytical separations.

The concept of VACNT membranes was initiated from atomic simulation studies. The transport diffusivities of light gases such as H_2 and CH_4 in carbon nanotubes and in zeolites were evaluated and compared, and it was found that transport rates in CNTs were orders of magnitude faster than that in zeolites. The exceptionally high transport rates result from the inherent smooth and frictionless nature of the interior of the nanotubes.[14–16] As a consequence, carbon nanotubes were proposed as one of the most promising membrane materials, predicted to have flux/selectivity properties far exceeding those of any other known inorganic materials. Hinds *et al.*[6] and Holt *et al.*[17] observed and confirmed the experimental high permeability of the CNT membranes by synthesising free-standing and silicon-chip supported VACNT membranes. The gas permeation fluxes were orders of magnitude higher than those predicted by the Knudsen model and the ideal gas selectivities were similar to Knudsen selectivity for non-hydrocarbon gases, and slightly higher than Knudsen selectivity for hydrocarbons. Lin *et al.*[18] also fabricated the VACNT membrane on a porous α-alumina supported by a multi-step method, and measured diffusivity values were about four times larger than the predicted values from the Knudsen diffusion model. Later, Falconer *et al.*[19] prepared high-density, vertically aligned carbon nanotube membranes *via* CVD followed by solvent evaporation. The gas permeability was 4–7 orders of magnitude higher than previous reports and approximately 450 times of those predicted by Knudsen diffusion. Meanwhile, the first data of mixture gas transport through single-walled carbon nanotube membrane was reported by Kim *et al.*,[20] confirming that non-Knudsen transport occurs in aligned CNT membrane.

By comparing the gas permeation results from the above references, it can be concluded that high areal density and small CNT inner diameter can facilitate permeation and improve separation performance. However, since the membranes were fabricated *via* different CNT alignment routes as well as interspace filling methods, it is difficult to directly compare the membrane performances. On one hand, the physical and chemical properties of vertically aligned carbon nanotubes, such as tube blockage by catalyst and substrate, as well as the degree of CNT graphitisation, are greatly influenced by the CVD methods and conditions. On the other hand, the membrane permeability is also affected by the membrane fabrication method, including CNT forest filling and cap removal routes. Therefore, it would be worthwhile to investigate both areal density and diameter effects on permeation performance for the

[a]*The University of Queensland, School of Chemical Engineering, Brisbane, 4072, Australia. E-mail: z.zhu@uq.edu.au (Z H Zhu); Fax: 61 7 3365 4199; Tel: 61 7 33653528*
[b]*Centre for Computational Molecular Science, The University of Queensland, Australian, Institute for Bioengineering and Nanotechnology (AIBN) Building 75, QLD, 4072, Brisbane, Australia*
[c]*The University of Queensland, School of Mechanical Engineering, Brisbane, 4072, Australia*

same CVD system and membrane fabrication procedure. Also, the temperature effect on aligned CNT membrane permeation behaviour has not been reported yet, although such work is necessary to study the non-Knudsen transport phenomenon.

In this study, we grew aligned carbon nanotubes *via* the *in situ* gas phase pyrolysis of a carbon source together with organometallic precursor, followed by membrane fabrication through filling the CNT gaps with epoxy monomer. Membranes with different CNT areal density and pore diameter were constructed by varying CVD parameters. The gas separation performance was studied and compared among these membrane samples, and discussion is provided regarding the CNT diameter, areal density and temperature effects on gas permeability.

2. Experimental section

2.1 Aligned carbon nanotube growth using camphor as carbon source

The growth of carbon nanotubes was conducted by CVD of a gas mixture of catalyst source (ferrocene) and carbon source (camphor) on a quartz substrate, using the pyrolysis apparatus, as outlined in an earlier study.[21] A two-stage furnace system fitted with a quartz tube (inner diameter: 47 mm, length: 1.1 m) was used as the reactor. The mixture of the ferrocene (Sigma-Aldrich, 99% pure) and camphor (Sigma-Aldrich, 99.5% pure) with a camphor/ferrocene weight ratio adjusted from 7.5 to 10 was put into a quartz boat and placed inside the first part of quartz tube. The commercial quartz substrates, which had been subjected to cleaning with acetone, were located in the second part of the quartz tube at measured distances from the boat. Before the CVD process, Ar gas (Coregas, 99.999%) was initially flowed through the tube reactor to remove the residue air as the second furnace was heated up to the CVD temperature, 900 °C. After the second furnace attained the CVD temperature, the camphor/ferrocene mixture was heated up in the first furnace with a heating rate of 15 °C min^{-1} until the temperature reached ~155 °C. Argon gas was then passed through the quartz tube at a flow rate of 1.1 L min^{-1} to blow the camphor/ferrocene mixture vapour into the second furnace. The concentration of water vapour in the gas flow was controlled by applying an argon stream passing through a water saturator at a flow rate of 5 ml min^{-1} with the corresponding concentration of water in gas flow of around 80 ppm. The thermal CVD was conducted at 900 °C for 30 min, and after that, the reactor was cooled to room temperature under pure Ar atmosphere with the moist argon switched off. A deposit of carbon was found on the substrates and tube inner surface.

2.2 Membrane fabrication

The inter-tube gaps of the as-synthesized CNT array on the quartz support were filled with the epoxy resin (LECO co. epoxy resin: 811-563-103, hardener: 812-519-haz, monomer: hardener = 100 : 14). Under vacuum the solvent-free low viscosity epoxy mixture penetrated into the aligned CNT matrix and filled up the gaps. The CNT/epoxy composite was degassed at room temperature for 1–2 days to remove any air bubbles and to allow curing. The surface of the coated CNT appeared transparent, indicating that the black CNT was completely covered by the epoxy over-layer. The membranes were removed from the quartz substrate by hydrofluoric acid and washed with deionised water followed by drying. A simple mechanical polishing method was used to remove the epoxy over-layer and to open the closed tips of CNTs. Specifically, a polishing machine (Buehler Vector Head/Beta Polishing Machine) and 600/2500-mesh sand papers were used to carefully sand off the surface of the CNT membrane disk. The sanding process continued until black CNTs appeared on the surface, and then further polishing was conducted to adjust the membrane thickness and ensure CNT cap removal. The sanded composite membranes were immersed in a 15% hydrochloride acid solution for about 1 day to ensure the removal of most of the catalyst residues. After that, the membranes were washed with the deionized water, followed by drying under vacuum. The derived epoxy-ACNT membranes are flat and crack free. The aligned carbon nanotube membranes derived from ferrocene/camphor ratio of 1 : 7.5 and 1 : 10 are denoted as VACNT-M1 and VACNT-M2, respectively.

2.3 Characterization

The morphologies of carbon nanotube arrays and the corresponding membranes were examined by scanning electron microscopy (SEM) with a JEOL JSM 6300 operated at 5 kV. The tortuosities can be calculated from the CNT length divided by the film thickness as follow:

$$\tau = \left(\frac{S}{L}\right)^2 \quad (1)$$

where S is the average actual length of about 20 fibers in straight line distance (μm). L is membrane thickness (μm).

High resolution transmission electron microscopy (HRTEM) was performed on a JEOL JEM-2100 microscope, with accelerating voltages of 200 kV. The samples were dispersed by sonication in ethanol, then deposited on a holey carbon TEM grid and dried. The aligned carbon nanotube membrane was glued on a porous stainless steel support (porosity >30%, pore size: ~30 μm, Metallic Membrane Co. of Nanjing University of Technology) and sealed with high vacuum sealant (Torr seal, Varian). The gas permeation experiments were carried out by using a variable feed pressure and the constant volume permeation system, described elsewhere.[22] A leak test was performed to check the O-ring seal, and the leakage flow rate was shown to be less than 5×10^{-10} mol m^{-2} s Pa. Before testing, the gas line and the cell were purged with target gas from cylinder and evacuated several times. Then the VACNT membranes were held under vacuum for approximately 5 min before being exposed to the selected gas at a specific pressure. Pure hydrogen, nitrogen, oxygen, argon, carbon dioxide or methane (99.99–99.999%, Coregas, Australia) was introduced to the upstream side of the membrane, and the pressure of both sides was measured by a pressure transducer (MKS, Baratron 722A). Both pressure transducers were connected to a computer for data logging. Tests were carried out by controlling the pressure of the feed stream to a desired value, and evacuating the permeate side to a vacuum pressure. The pressure gradient was ensured to remain constant before measuring. The permeate stream valve was then closed allowing pressure to increase in the

permeate reservoir due to gas permeation though the membrane. The collected data was used to calculate the permeance according to eqn (2),

$$P = \frac{d}{d_t}\left(\ln\left(\frac{P_f - P_{p,0}}{P_f - P_{p,t}}\right)\right)\cdot\frac{V_p}{ART} \quad (2)$$

where P is the permeance (mol s^{-1} m^{-2} Pa^{-1}), P_f is the pressure of the feed side (Pa), $P_{p,0}$ is the initial pressure at the permeate side (Pa), $P_{p,t}$ is the transient pressure measured in the permeate volume (Pa), V_p (m^3) is the constant permeate reservoir volume, A is the permeable membrane area (m^2), R is the ideal gas constant (J mol^{-1} K^{-1}), and T is T/K. Each gas was tested for three times and the average value was reported. The ideal selectivity for two gases is determined by the permeance ratio.

3. Results and discussion

3.1 Characterizations of vertically aligned CNT arrays

Fig. 1 shows the cross section of as-grown multi-walled CNT arrays derived from different ferrocene concentrations. The CNT arrays show high degree of vertical alignment and are well packed to form a uniform carpet-style forest with a thickness of ~500 and ~215 μm for a camphor/ferrocene ratio of 7.5 and 10, respectively. High magnification images are also given in Fig. 1b and Fig. 1d, showing that most of carbon nanotubes are parallel to each other and quite straight. Near-unity tortuosities were estimated to be 1.1 ± 0.1 and 1.3 ± 0.3 by eqn (1) for two VACNTs samples. The density of VACNT arrays is ~10^{10} nanotubes cm^{-2}, and varies with the mass ratio of camphor to ferrocene. The ferrocene quantity in the mixed precursor determines the Fe catalyst concentration in the mixed precursor gases and therefore leads to variation of both Fe catalyst density and Fe nanoparticle sizes on the substrate. Higher ferrocene concentrations result in denser catalyst packing and straighter nanotubes but larger catalyst particles due to nano-Fe particle agglomeration.[23]

The typical TEM images of CNTs derived from different camphor/ferrocene ratios are shown in Fig. 2. Most of the tubes

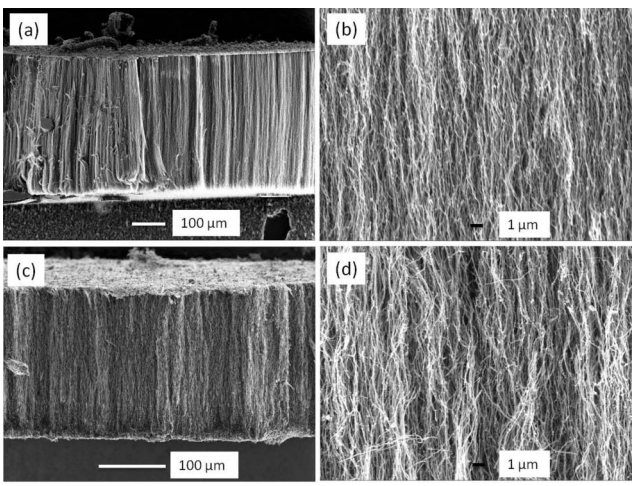

Fig. 1 Cross-sectional morphology of aligned CNT arrays (a,b: camphor/ferrocene = 7.5, c,d: camphor/ferrocene = 10).

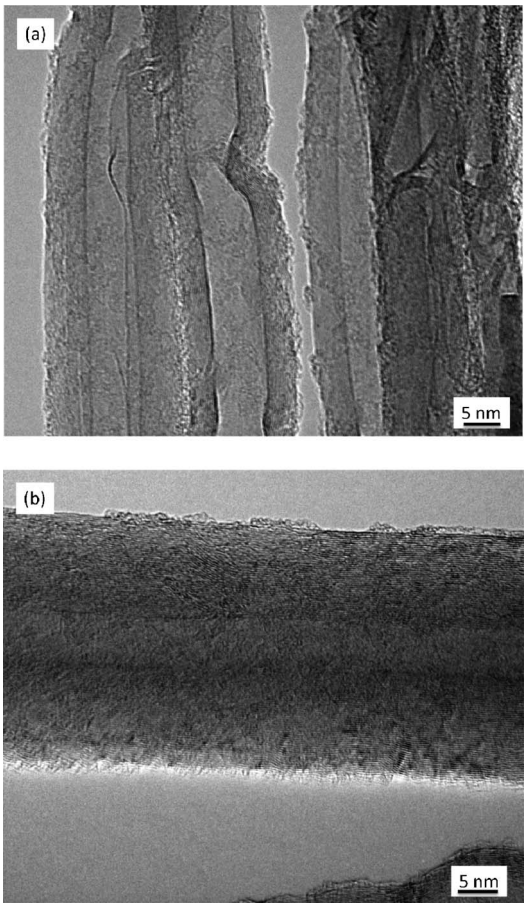

Fig. 2 HRTEM image of carbon nanotubes derived from various camphor/ferrocene mass ratio (a: 7.5, b:10).

are quite straight and continuously hollow, but some bamboo structures and bridged tube walls can also be observed. As can be seen in Fig. 2a, CNTs grown from higher ferrocene concentration (camphor/ferrocene = 7.5) have larger average inner diameter (7.7 nm), while a smaller inner diameter of around 5.1 nm was obtained by reducing the ferrocene amount (camphor/ferrocene = 10) in Fig. 2b. The increase of inner diameter size can be attributed to the larger Fe catalyst particle size.[24] In addition, some thin tubes with less than 2 nm diameter can also be seen among the aligned tubes due to non-uniform catalyst distribution.

3.2 Characterizations of vertically aligned CNT membranes

As reported in the references, VACNT membranes have previously been formed by filling the carbon nanotube interspace with a polymer or ceramic matrix, such as polystyrene,[6,18] polysulfone[20] and silicon nitride.[17] In this study, the as-synthesized aligned carbon nanotube arrays are relatively thick (>200 μm) and thus generate larger diffusion resistance for polymer filling. Consequently, to achieve complete filling of the CNT interspaces smaller monomer molecules are preferred, instead of filling using larger molecules. In this work, the dense membranes were fabricated by filling with epoxy, which has been shown to be a practicable route to fill super long VACNT arrays.[25] Freestanding membranes are produced after the quartz

substrate base is removed. The typical cross-section and surface morphologies of the CNT membrane are shown in Fig. 3. The thickness of the VACNT-M2 membrane is around 105 μm (Fig. 3a) with the aligned CNTs intact. Noting that the membrane thickness of the original ACNT arrays is ~215 μm (Fig. 1b), it is apparent that mechanical polishing removes almost half of the carbon nanotube carpet. The process ensures that both ends of the CNTs are opened and the nano-scale channels of carbon nanotubes are exposed. The thickness variation and polished fragments can also be observed in Fig. 3a, which are attributed to the surface roughness on membrane caused by the mechanical polishing. Fig. 3b shows that a dense structure is formed by polymer filling into the CNT spacing, *i.e.* the nanotube carpet is fully impregnated without voids. Some highly curved CNTs apparent in Fig. 3b are caused by cutting. Mechanical polishing does not affect the membrane integrity and dense structure, only leading to higher surface roughness, as can be seen in Fig. 3c.

Fig. 4 shows the polished surface of aligned carbon nanotube membranes for evaluating areal density. Some broken carbon nanotubes on the polymer surface can be observed after polishing, along with some pin holes in the polymer. The tips of the CNTs are removed by polishing and leave most of the carbon nanotube channels open and hollow for gas transportation. From the top-view images of VACNT membranes (Fig. 4), the number of observed nanotubes was counted in the given area (300 nm × 300 nm) to give an estimated areal density. The areal density of the aligned carbon nanotubes in membrane samples can be estimated as $\sim(1.1 \pm 0.2) \times 10^{10}$ and $\sim(6.7 \pm 1.2) \times 10^{9}$ nanotubes per cm^2, for samples derived from camphor to ferrocene mass ratio of 7.5 and 10, respectively. Fig. 5 shows some typical HRTEM pictures of carbon nanotubes after mechanical polishing. An open ended carbon nanotube with the carbon cap and tip catalyst removed is shown in Fig. 5a. However, as can be seen in Fig. 5b, in some cases graphitic shells block the nanotube and form bamboo morphology. Moreover, during CVD process, some catalyst particles migrate into the inner channel of CNT (Fig. 5c). Even though acid wash can remove most of the confined Fe catalysts, some residual catalysts

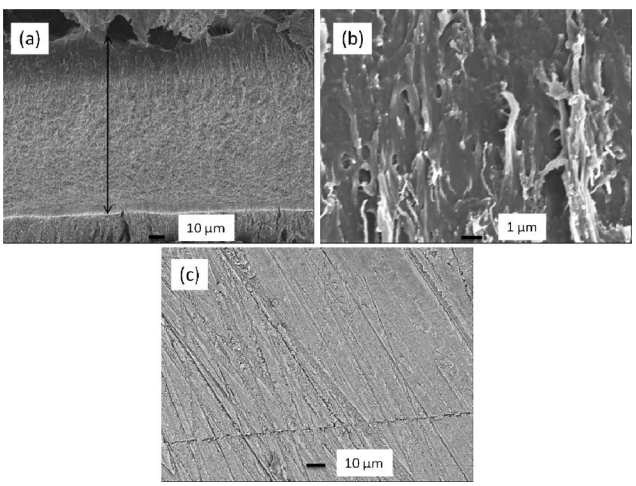

Fig. 3 SEM images of VACNT-M2 membranes with tube gap filled by Epoxy after polishing (a, b: cross-section; c: surface).

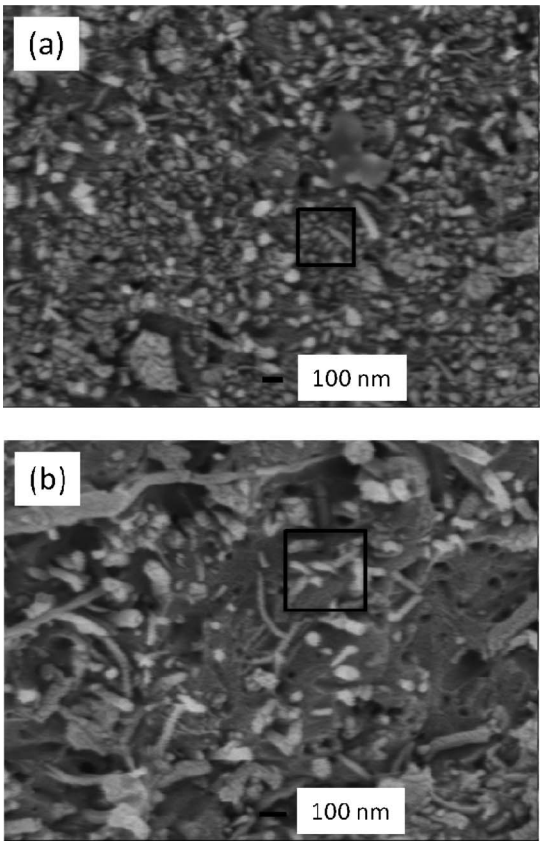

Fig. 4 SEM images of top surface of CNT membranes after mechanical polishing (a: VACNT-M1, b: VACNT-M2).

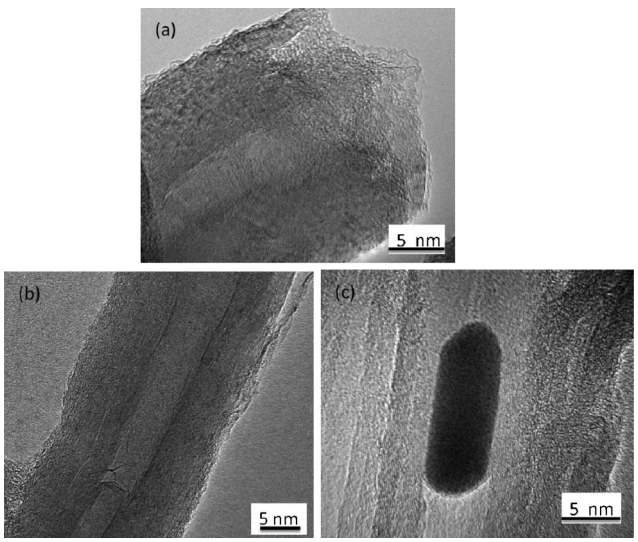

Fig. 5 (a) Typical HRTEM image for the tip removed CNT by mechanical sanding (b) Bamboo structure CNT (c) iron catalyst migrated into the channel.

may still remain in some channels and block the gas transport path, therefore limiting the molecular transport to some extent. It is noteworthy that more catalyst residues and bamboo structures were found in VACNT-M1 due to the higher ferrocene loading during the CVD process (figures not shown here).

3.3 Gas permeation performance of vertically aligned CNT membranes

Table 1 shows the hydrogen permeances for VACNT membranes at different preparation stages. Compared to the VACNT membranes, much higher permeability of the porous stainless steel support indicates that the diffusion resistance of the support can be neglected. The epoxy filled VACNT membranes without polishing possess CNTs with closed ends and covered with polymer, and therefore show very low hydrogen permeance as expected, around 10^{-10} mol m^{-2} s^{-1} Pa^{-1}. This means that there are essentially no channels through the membranes, and the permeance reflects gas diffusion in the epoxy polymer or perhaps tiny permeance from cross-membrane leakage. This confirms that the membranes are defect-free and the CNT gaps are fully filled, which is consistent with SEM images (Fig. 3). After reducing membrane thickness and removing the epoxy over-layer as well as the closed CNT tips by mechanical polishing, the hydrogen permeance increases dramatically by around two orders of magnitude. This dramatic permeance increment proves that gas diffusion resistance of polymer layer is much higher than carbon nanotube channel. Further permeance improvement is observed after acid washing, which means that catalyst residues are cleaned by acid and more unimpeded channels are provide for gas transportation.

The parameters of the VACNT membranes from different CVD conditions were given in Table 2 for calculating the Knudsen permeance and for comparison. The mean free path of gases at room temperature (~67 nm) is almost one order of magnitude larger than the pore diameter of the given VACNT membranes (5~8 nm). Therefore, the gas transportation through the VACNT membranes is expected to be in the Knudsen range. The calculated areal porosity in this study is similar to the doubled-walled VACNT membranes (5.0×10^{-3})[17] and multi-walled VACNT membranes (1.0×10^{-3})[7] from CVD synthesis, but is higher than the VACNT membrane grown from porous alumina support (6.2×10^{-4})[18] and membrane fabricated by filtration (7.9×10^{-4})[20] yet lower than high dense VACNT membrane (0.21).[19]

Table 1 Gas permeance for VACNT membranes (Pressure gradient: 2 atm, 25 °C)

	H_2 permeance (mol m^{-2} s^{-1} Pa^{-1})
Porous stainless steel support	~10^{-3}
Supported epoxy filled VACNT membrane	~10^{-10}
Supported VACNT membrane with both side polished	~10^{-8}
Supported polished VACNT membrane after HCl treatment	10^{-7}–10^{-6}

Table 2 Parameters of as-obtained VACNT membranes

	Parameters VACNT-M1	VACNT-M2
CNT structure	Multi-walled	Multi-walled
Ferrocene to Camphor ratio	1 : 7.5	1 : 10
CNT membrane thickness after polishing (μm)	~110 μm	~105 μm
CNT areal density (/cm^2)	~$(1.1 \pm 0.2) \times 10^{10}$	~$(6.7 \pm 1.2) \times 10^9$
Average pore diameter (nm)	7.7	5.1
CNT tortuosity factor (τ)	~1.1	~1.3
Areal porosity (ε)	0.0057	0.0016

The permeability and diffusivity in Knudsen flow range can be estimated from eqn (3,4)[7,18]

$$P_K = \frac{2\varepsilon r}{\tau RTL}\left(\frac{8RT}{\pi M}\right)^{\frac{1}{2}} \quad (3)$$

$$D_K = \left(\frac{2}{3}\right)\left(\frac{8RT}{\pi M}\right)^{\frac{1}{2}} r \quad (4)$$

where P_K is the Knudsen permeability (mol m^{-2} s^{-1} Pa^{-1}), D_K is Knudsen diffusivity (m^2 s^{-1}), M is molecular weight of penetrant (kg mol^{-1}), R is the universal gas constant (J mol^{-1} K^{-1}), T is absolute T/K, r is the inner diameter of CNT (m), L is the membrane thickness (m), ε is the porosity and τ is the tortuosity.

The permeance enhancement factor (α) can be calculated by the following equation:

$$\alpha = \frac{P}{P_K} \quad (5)$$

Membranes with high separation performance should not display any viscous flow, in which case the permeability is independent of the feed pressure (eqn (3)). When viscous flow does occur, the permeability increases with increasing pressure gradient.[26] Argon gas permeation tests under various pressure gradients were carried out to examine polymer filling and membrane integrity. In Fig. 6, the Ar permeation flux *versus* average pressure is constant irrespective of the pressure gradient demonstrating the absence of larger cracks or cross membrane pore big enough for viscous flow through the VACNT membranes.

Based on Knudsen diffusion, the gas selectivity is proportional to square root of the inverse ratio of the molecular weights. For instance, the ideal gas selectivity of hydrogen to methane is 2.83. The hydrogen selectivities *versus* other gases are shown in Fig. 7,

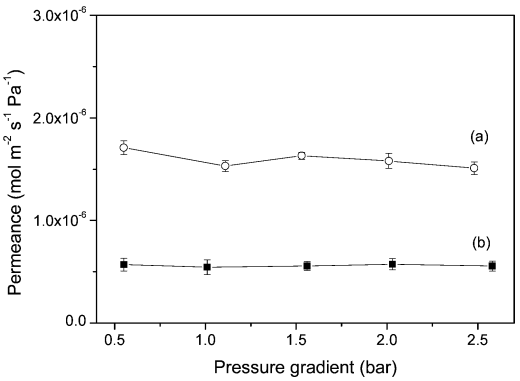

Fig. 6 Argon permeances through vertically aligned carbon nanotube membranes at 20 °C (a. VACNT-M1, b. VACNT-M2).

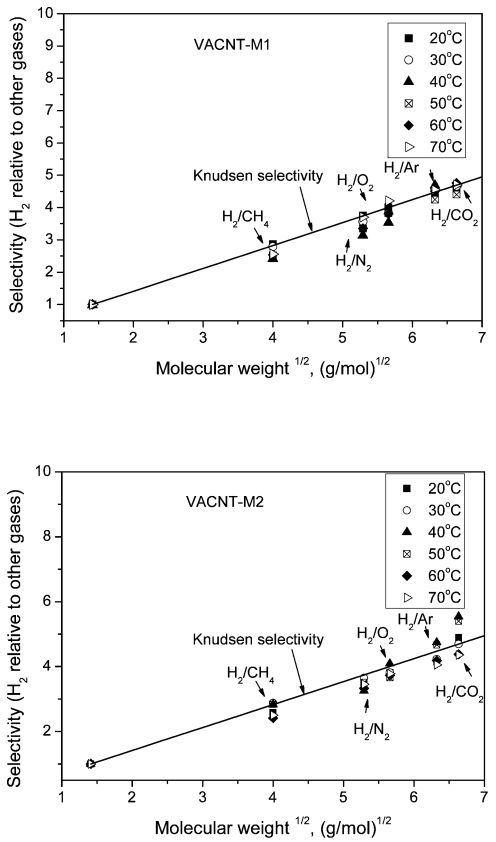

Fig. 7 Hydrogen selectivity relative to other gases (pressure gradient: 2 atm).

in which the measured values are scattered around the Knudsen selectivity regime. On the other hand, for Knudsen diffusion, selectivity should be independent of temperature, so selectivity changes at different temperatures indicate the presence of diffusion processes apart from Knudsen, such as surface diffusion. Surface diffusion along carbon nanotube walls may play a significant role in gas transportation and result in deviation from the ideal Knudsen gas separation behaviours.[15,27]

The membrane permeance and enhancement factor over Knudsen diffusion for each gas are shown in Fig. 8. Based on the enhancement factor (eqn (5)), the permeation fluxes are much higher than the Knudsen diffusion, which confirms that the gas transport happens primarily through the carbon nanotube channel rather than the dense polymer matrix. In Fig. 8c,d, the permeation enhancement phenomenon is consistent with experimental observations of carbon nanotube membranes reported previously.[4,6,7,17–19] The enhancement factors are 30–60 for VACNT-M1 and 30–80 for VACNT-M2 at room temperature. Such high diffusion enhancements can be attributed to the smooth interior channels in the VACNT membranes in which molecular collisions do not have any backscattering, and keep all forward momentum upon reflections down the CNT channels.[7] The skate-down gas molecular route along the tube channel differs from randomly-scattered Knudsen diffusion and therefore generates very high flow velocity.[15] This specular momentum transfer significantly increases the diffusivities, to an extent much higher than kinetic theory.[14,28,29] Comparing the enhancement factors for the two membranes (Fig. 8c and d), the smaller-sized

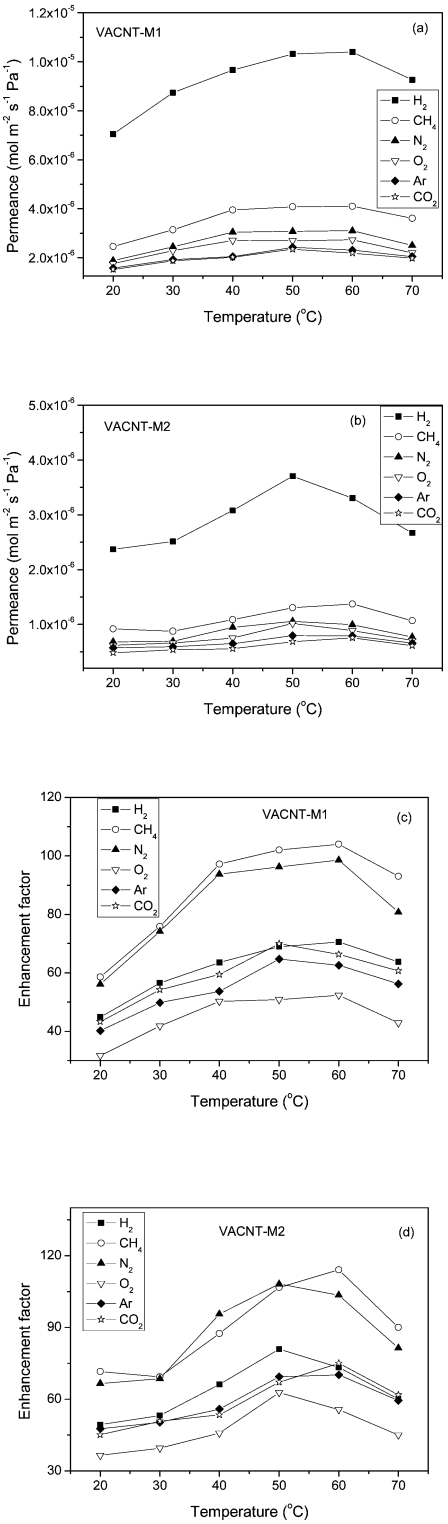

Fig. 8 (a, b) Permeance of gases through different aligned carbon nanotube membranes and (c, d) enhance factor over Knudsen diffusion for each gas.

VACNT-M2 exhibits a slightly higher enhancement factor than VACNT-M1 with larger tube channels. This difference in permeance enhancement is most likely related to the various catalyst residue amounts in the two membrane samples. Since

more catalyst residue is found in VACNT-M1 than VACNT-M2, it is likely that more tube blockage occurred. Hence, though higher permeance arises by increasing the areal density of carbon nanotubes by increasing the catalyst precursor concentration in the CVD process, a resulting higher catalyst residue amount may also bring more tube blockage. Therefore, it can be deduced that there exists an optimum catalyst concentration for membrane permeance, balancing the requirements of both CNTs areal density and unblocked channels.

According to the Knudsen equation (eqn (3)) permeance would decrease with increasing temperature. However, in this study, the permeances of both VACNT membranes first increase with increasing temperature up to 50–60 °C, and then drop off gradually. This permeance behaviour with temperature, taken together with the enhanced diffusion rate, illustrates that the gas diffusion in CNT channels does not fully obey the Knudsen diffusion law and there are likely other diffusion mechanisms making contributions to the gas diffusion. In general, the gas transport through mesoporous membrane materials arises from viscous diffusion, Knudsen diffusion and surface diffusion.[30] The thermally activated diffusion process below 60 °C and the different enhancement factors of various gases that are observed in this study and in reference,[7] implies that the interaction between gases and carbon nanotube walls affects the total gas diffusivity. It may be speculated that gas adsorption on the inner wall of CNTs could occur at low temperature and generate slow surface diffusion layers. The effect of this surface diffusion layer on bulk diffusion becomes more significant in thinner tubes than larger tubes. In the VACNT membranes, though the average tube diameter is in the mesopore range, some micropores still exist due to small diameter tubes (<2 nm), carbon layer distortion and catalyst blockage. In this case, the surface adsorption diffusion cannot be neglected and will affect the overall permeability. In some microporous membranes, the surface-adsorption-based diffusion shows the activation process and follows an Arrhenius-type mechanism.[31,32] The activated permeation can be described by

$$P_i^{\circ} = P_i^{*} e^{-\frac{E}{RT}} \quad (6)$$

P_i° is the measured pure gas permeance through the membrane, P_i^{*} is the value of P_i° at infinite temperature, E is the activation energy.

Eqn (6) shows that the thermal activated permeance tends to be enhanced with rising temperature. However, such surface-adsorption diffusion is also affected by physisorption, which will be weakened by elevating temperature, leading to a smaller contribution of surface-adsorption diffusion to the total diffusion at higher temperature. After the surface physisorption become attenuated by heating, the permeance starts to go down with further temperature increases, following the Knudsen diffusion mechanism. In this case, a maximal permeance can be observed.

On the other hand, by reducing the pore size or through surface modification, the surface-adsorption diffusion layers may be induced to occupy a larger proportion of the diffusion channels. This dominating surface-adsorption diffusion mechanism can enhance the separation selectivity by preferential adsorption of certain components on the pore surfaces.[32] Therefore, it can be proposed that the separation efficiency of membranes can be altered by both pore size control and by tailoring the physico-chemical nature of the pore surface. Specifically, a VACNT membrane with higher separation performance can be realized by surface modification on the CNT interior channels or by making thinner tubes, such as single-walled carbon nanotubes.

4. Conclusions

In summary, the vertically-aligned carbon nanotube membranes have been fabricated *via* a gas phase catalytic CVD process followed by epoxy encapsulation. Open-ended CNT and exposed hollow tube channels are achieved by mechanic polishing and acid wash. Aligned carbon nanotubes with different tube inner diameter and areal density are tuned by the catalyst precursor content. Based on the gas permeation results of the corresponding membranes, the gas permeability is much higher than the Knudsen permeability, the enhancement factors of small-sized VACNT membranes are higher (30–80, 20 °C) than the membrane with larger tubes (30–60, 20 °C). While the hydrogen selectivities are all in the Knudsen range. To investigate the temperature dependence of permeability, the hydrogen selectivity still follows the Knudsen predication as increasing membrane operation temperature, while the permeance peaks around 50–60 °C. This deviated phenomenon confirms the existence of non-Knudsen transport and thermally activated diffusion process. The differences of permeance increment and enhancement factor for various gases may be attributed to the surface adsorption diffusion. Based on the results in this study, it can be proposed as an effective way to achieve better membrane performance by increasing areal density, decreasing catalyst contamination and operating at an optimum temperature. The gas selectivity is also expected to be varied by reducing the tube diameter or applying inner surface modification. However, the non-Knudsen diffusion in the CNT membranes still requires to be figured out by both modelling and experimental work.

Acknowledgements

The financial support by Australian Research Council (ARC) discovery project is greatly appreciated. The first author also likes to acknowledge the support from IPRS (Endeavour International Postgraduate Research Scholarship, Australia), UQRS (University of Queensland Research Scholarship).

References

1 W. A. de Heer, A. Chaelain and D. Ugarte, *Science*, 1995, **270**, 1179.
2 W. A. de Heer, J. M. Bonard, K. Fauth, A. Châtelain, D. Ugarte and L. Forró, *Adv. Mater.*, 1997, **9**, 87.
3 E. J. Garcia, B. L. Wardle and A. John Hart, *Composites, Part A*, 2008, **39**, 1065.
4 M. Majumder, N. Chopra, R. Andrews and B. J. Hinds, *Nature*, 2005, **438**, 44.
5 A. Misra, J. Giri and C. Daraio, *ACS Nano*, 2009, **3**, 3903.
6 B. J. Hinds, N. Chopra, T. Rantell, R. Andrews, V. Gavalas and L. G. Bachas, *Science*, 2004, **303**, 62.
7 M. Majumder, N. Chopra and B. J. Hinds, *ACS Nano*, 2011, **5**, 3867.
8 S. A. Miller and C. R. Martin, *J. Am. Chem. Soc.*, 2004, **126**, 6226.
9 S. A. Miller, V. Y. Young and C. R. Martin, *J. Am. Chem. Soc.*, 2001, **123**, 12335.

10 A. I. Lopez-Lorente, B. M. Simonet and M. Valcarcel, *Anal. Chem.*, **82**, 5399.
11 B. Suarez, Y. Moliner-Martinez, S. Cardenas, B. M. Simonet and M. Valcarcel, *Environ. Sci. Technol.*, 2008, **42**, 6100.
12 A. S. Brady-Estévez, S. Kang and M. Elimelech, *Small*, 2008, **4**, 481.
13 M. Majumder, N. Chopra and B. J. Hinds, *J. Am. Chem. Soc.*, 2005, **127**, 9062.
14 D. M. Ackerman, A. I. Skoulidas, D. S. Sholl and J. K. Johnson, *Mol. Simul.*, 2003, **29**, 677.
15 A. I. Skoulidas, D. M. Ackerman, J. K. Johnson and D. S. Sholl, *Phys. Rev. Lett.*, 2002, **89**, 185901.
16 A. I. Skoulidas, D. S. Sholl and J. K. Johnson, *J. Chem. Phys.*, 2006, **124**, 054708.
17 J. K. Holt, H. G. Park, Y. Wang, M. Stadermann, A. B. Artyukhin, C. P. Grigoropoulos, A. Noy and O. Bakajin, *Science*, 2006, **312**, 1034.
18 W. Mi, Y. S. Lin and Y. Li, *J. Membr. Sci.*, 2007, **304**, 1.
19 M. Yu, H. H. Funke, J. L. Falconer and R. D. Noble, *Nano Lett.*, 2009, **9**, 225.
20 S. Kim, J. R. Jinschek, H. Chen, D. S. Sholl and E. Marand, *Nano Lett.*, 2007, **7**, 2806.
21 M. Kumar and Y. Ando, *Chem. Phys. Lett.*, 2003, **374**, 521.
22 L. Ge, Z. Zhu and V. Rudolph, *Sep. Purif. Technol.*, 2011, **78**, 76.
23 M. A. Signore, A. Rizzo, R. Rossi, E. Piscopiello, T. Di Luccio, L. Capodieci, T. Dikonimos and R. Giorgi, *Diamond Relat. Mater.*, 2008, **17**, 1936.
24 C. L. Cheung, A. Kurtz, H. Park and C. M. Lieber, *J. Phys. Chem. B*, 2002, **106**, 2429.
25 F. Du, L. Qu, Z. Xia, L. Feng and L. Dai, *Langmuir*, 2011, **27**, 8437.
26 Y. S. Lin and A. J. Burggraaf, *J. Membr. Sci.*, 1993, **79**, 65.
27 C. Matranga, B. Bockrath, N. Chopra, B. J. Hinds and R. Andrews, *Langmuir*, 2006, **22**, 1235.
28 G. Arya, H.-C. Chang and E. J. Maginn, *Mol. Simul.*, 2003, **29**, 697.
29 G. Arya, H.-C. Chang and E. J. Maginn, *Phys. Rev. Lett.*, 2003, **91**, 026102.
30 E. L. Cussler, *Diffusion: Mass transfer in fluid systems*, *Cambridge Univ Pr*, 1997.
31 A. B. Fuertes, *J. Membr. Sci.*, 2000, **177**, 9.
32 M. B. Rao and S. Sircar, *J. Membr. Sci.*, 1993, **85**, 253.